ELSEVIER

Materials Science and Engineering B 139 (2007) 201–208

MATERIALS SCIENCE & ENGINEERING B

www.elsevier.com/locate/mseb

Synthesis and photocatalytic performance of $ZnWO_4$ catalyst

Guangli Huang, Yongfa Zhu *

Department of Chemistry, Tsinghua University, Beijing 100084, PR China

Received 13 November 2006; received in revised form 15 February 2007; accepted 17 February 2007

Abstract

$ZnWO_4$ powder photocatalyst was prepared by calcining co-precipitated precursor, and its high photocatalytic activity was revealed. The $ZnWO_4$ crystal phase was formed at 450 °C for 4 h. The crystal size and particle size of $ZnWO_4$ powder increased with the increasing of calcination temperature and time. At 500 °C for 4 h, the photocatalyst reaches the highest photocatalytic activity with formaldehyde removal efficiency of 90% within 25 min. Moreover, its photocatalytic activity is almost similar to that of P-25 in degradation of gaseous formaldehyde. $ZnWO_4$ also displayed high photocatalytic activity in aqueous solution for degradation of RhB. The high crystallinity and large surface area are responsible for its high photocatalytic activity.

Keywords: $ZnWO_4$; Photocatalytic; Calcination; Co-precipitated precursor

1. Introduction

Photocatalytic degradation of organic compounds for the purpose of purifying wastewater from industries and households has attracted much attention in recent years [1–3]. It has been reported that TiO_2 [4], Ta_2O_5 [5], $Na_2W_4O_{13}$ [6], $Bi_2W_2O_9$ [6], $(NaBi)_{0.5}WO_4$ [7], $AgInW_2O_8$ [8], Bi_2WO_6 [9–11], etc. show favorable photocatalytic activity under ultraviolet or visible light irradiation. In the past decade, $ZnWO_4$ have attracted much attention because of its magnetic, scintillated, luminescent and catalytic properties [12]. $ZnWO_4$ has the monoclinic wolframite structure with C_{2h} point group symmetry and $P2/c$ space group. The structure of $ZnWO_4$ comprises infinite zigzag chains, running parallel to [0 0 1], of either edge-sharing ZnO_6 octahedron or edge-sharing WO_6 octahedra. Each chain of ZnO_6 octahedra is corner-linked to four chains of WO_6 octahedra and vice versa, leaving open channels which are also parallel to [0 0 1]. Within the network of hexagonally close-packed O atoms, Zn and W atoms are ordered on the octahedral interstices such that layers of O, W, O, Zn, O... are formed, and these are interlayered with cation-absent layers. The ZnO_6 and WO_6 octahedra consist of three pairs of cation–oxygen bonds with Zn and W atoms being displaced from the centre of their octahedral by approximately 0.29 and 0.32 Å, respectively, along [0 1 0] [13]. Bi_2WO_6 has been reported as a good photocatalyst for water splitting and photo-degradation of organic compounds under visible light irradiation [9–11], which possess layered structure with the perovskite-like slab of WO_6 [14]. Recently, we have reported $ZnWO_4$ exhibited the high photocatalytic activity for the decomposition of both the aqueous RhB and gaseous formaldehyde under UV light irradiation [15]. Moreover, we also found that $ZnWO_4$ films explored photoelectrochemical properties [16]. On the above basis, it is reasonable to believe that $ZnWO_4$ may be a promising materials applied in photocatalysis and photovoltaic cells.

Obviously, the suitable synthetic approaches may give rise to differing photochemical properties due to possible variation of morphology and sizes. $ZnWO_4$ has thus far been prepared by several different processes such as Czochralski method, solid-state metathesis reaction and sol–gel method [17]. However, $ZnWO_4$ samples were essential to perform at high temperature, and the photocatalytic activities were not high due to large crystal and low surface area. Some new attempts have been done about synthesis of $ZnWO_4$ by using hydrothermal method to obtain high surface area [12,15,18].

Here, we report another new method for preparation of $ZnWO_4$ powders from co-precipitation precursor. The advantages of this method are easy to form the complex oxide at relative low calcination temperature, short calcination time and easy to dope. To our knowledge, still no literature reports the preparation of $ZnWO_4$ photocatalysts using this method. In this paper, $ZnWO_4$ photocatalyst prepared via co-precipitation

* Corresponding author. Tel.: +86 10 62783586; fax: +86 10 62787601.
E-mail address: zhuyf@mail.tsinghua.edu.cn (Y. Zhu).

0921-5107/$ – see front matter © 2007 Elsevier B.V. All rights reserved.
doi:10.1016/j.mseb.2007.02.009

exhibited high photocatalytic activity. The effect of various preparation conditions including temperature and time on the microstructure, surface area and photocatalytic capability of the $ZnWO_4$ powders was investigated in details.

2. Experimental

2.1. Synthesis

$ZnWO_4$ were prepared through calcination co-precipitation precursor process. All chemicals used were analytic grade reagents without further purification. The start materials were corresponding $Zn(NO_3)_2{\cdot}6H_2O$ and $Na_2WO_4{\cdot}2H_2O$ in 1: 1 molar ratio. The start materials were mixed together; and 100 mL distilled water was added. White precipitates appeared immediately, and the beaker was putted in ultrasonic bath for 30 min in order to complete the precipitate reaction. The precipitates were filtered off, washed several times with distilled ethanol, and dried at 100 °C for 4 h in air, subsequently, the collected precipitated were calcined for 4 h at 400 °C, 450 °C, 500 °C, 550 °C, 600 °C or calcined at 500 °C for 1 h, 2 h, 4 h, 8 h, 16 h, respectively.

2.2. Characterization

The products were characterized by powder X-ray diffraction (XRD) on Bruker D8-advance X-ray diffractometer at 40 kV and 40 mA for monochromatized Cu Kα ($\lambda = 1.5418$ Å) radiation. Infrared transmission spectra were recorded for KBr disks containing the powder sample with an FT-IR spectrometer (Perkin-Elmer 1600). Morphologies of the prepared samples were further examined with transmission electron microscopy (TEM) by a JEM 1010 electron microscope operated at an accelerating voltage of 120 kV. BET surface area was determined by ASAP 2010 V5.02H. The absorbed gas was nitrogen. UV–vis diffuse reflectance spectrums (DRS) of the samples were measured by using Hitachi U-3010 UV–vis spectrophotometer.

2.3. Photocatalytic test

Photocatalytic activities of $ZnWO_4$ powders were evaluated by degradation of rhodamine-B (RhB) and gaseous formaldehyde under ultraviolet light irradiation of 11 W low-pressure lamp with 254 nm, respectively. The average light intensity was 1.0 mW cm^{-2}. The radiant flux was measured with a power meter from Institute of Electric Light Source (Beijing). RhB solutions (200 mL, 10^{-5} mol L^{-1}) containing 0.1 g of $ZnWO_4$ powders were put in a glass beaker. Before the light was turned on, the solution was first ultrasonicated for 10 min, and then stirred for 30 min to ensure equilibrium between the catalyst and the solution. Three millilitres of samples were taken at given time intervals and separated through centrifugation (4000 rpm, 10 min). The supernatants were analyzed by recording variations of the absorption band maximum (553 nm) in the UV–vis spectra of RhB by using a U-3010 spectrophotometer (Hitachi).

The photocatalytic activity experiments on $ZnWO_4$ powders for oxidation decomposition of formaldehyde in air were performed at ambient temperature using a sealed reactor. The photo-reactor used was a 250 mL cylindrical quartz vessel, which consisted of an inlet, an outlet and a sample port. The photocatalysts were prepared by coating an aqueous suspension of $ZnWO_4$ powders onto the glass plate with diameters of 7.5 cm × 2.5 cm areas homogeneously. The weight of the photocatalyst used for each experiment was kept at about 0.050 g. The $ZnWO_4$ photocatalysts were dried in an oven at 100 °C for about 2 h and then cooled to room temperature before use. After the film coat with $ZnWO_4$ powder photocatalysts were placed in the reactor. An amount of formaldehyde mixed with air was injected into the reactor. The reactor was connected to a dryer containing $CaCl_2$ that was used for controlling the initial humidity in the reactor. The formaldehyde vapor was allowed to reach adsorption equilibrium with catalysts in the reactor in the dark prior to UV light irradiation. The initial concentration of formaldehyde after adsorption equilibrium was controlled to 1200 ± 10 ppm for all experiments, which remained constant for about 2–3 min until a 11-W, 254 nm UV lamp in the reactor was switched on. The initial concentration of water vapor was 1.20 ± 0.01 vol.%, and the initial temperature was 25 ± 1 °C. During the photocatalytic reaction, the formaldehyde concentration decreased steadily with an increase in UV illumination time. Each reaction was followed for 60 min. Subsequently, 1 mL of gas in the photo-reactor was taken at 5 min intervals. The concentration of obtained formaldehyde was measured with a SP-502 gas chromatograph (GC) equipped with a flame ionization detector and a 2 m stainless-steel column (GDX-403) at 100 °C.

The photocatalytic activity of the samples can be quantitatively by comparing the removal efficiency of formaldehyde ($R(\%)$). $R(\%)$ was calculated according to the following equation [19]:

$$R(\%) = \frac{[\text{gas}]_0 - [\text{gas}]_t}{[\text{gas}]_0} \times 100\%$$

where $[\text{gas}]_0$ and $[\text{gas}]_t$ represent the initial equilibrium concentration and reaction concentration of formaldehyde, respectively.

3. Results and discussion

3.1. Formation process of $ZnWO_4$ crystalline phase

Calcination is a common treatment that can be used to improve the crystallinity [20]. The influence of the calcination temperature on the formation of $ZnWO_4$ crystalline phase has been investigated using XRD. Fig. 1(a) shows XRD patterns of as-prepared samples calcined at different temperatures from 400 to 600 °C. It was found that the precursor was amorphous. At 400 °C for 4 h, the resultant powders were dark brown, denoting the intergradation of $ZnWO_4$. It is attributed to contain a lot of carbons from precursor, which was washed with ethanol. At 450 °C for 4 h, a pure $ZnWO_4$ crystal structure could be appeared. With increase of calcination temperature, all the peaks were intensified and became sharper without phase transformation. After calcining at 500 °C for 4 h, the most intense peaks at $2\theta = 30.5°$ are divided into three factions, which is clearly recognized by obvious separation among 1 1 1, −1 1 1 and 0 2 0 lines.

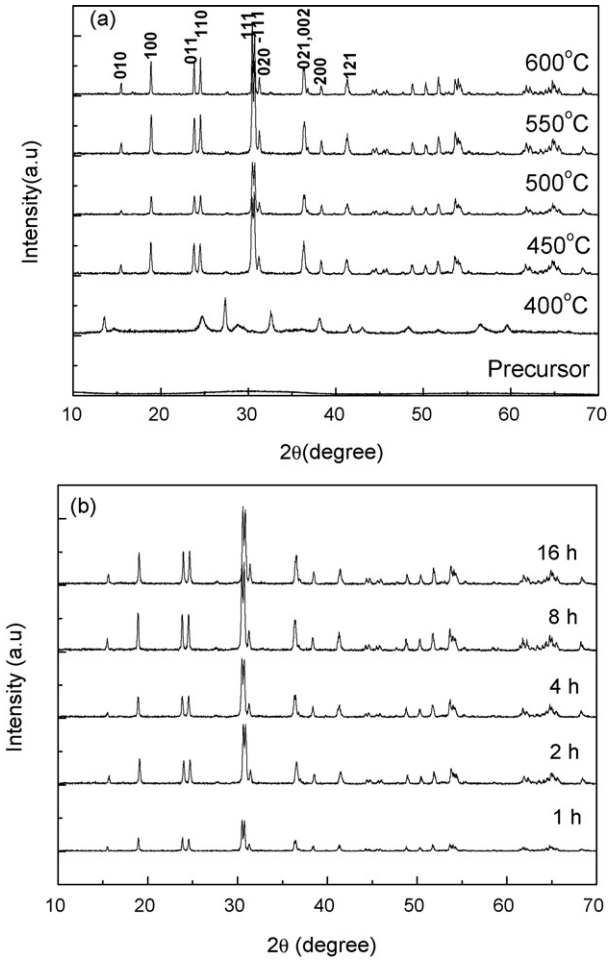

Fig. 1. XRD patterns of as-prepared samples calcined: (a) various temperatures for 4 h; (b) various times at 500 °C.

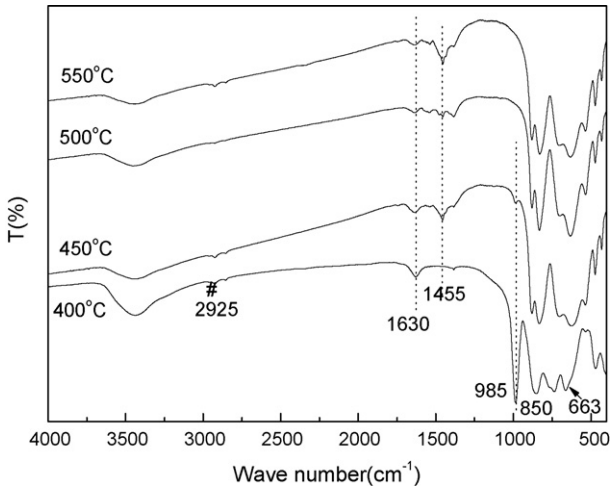

Fig. 2. FT-IR spectra of the $ZnWO_4$ powder samples calcined at various temperatures for 4 h.

This result demonstrates that high calcination temperature was favorable to the formation of $ZnWO_4$ crystals.

The influence of calcination time on the formation of $ZnWO_4$ crystalline phase was also studied by XRD. As it was shown in Fig. 1(b), the crystalline increased with extension of calcination time. However, the influence of calcination temperature was more significant than that of calcination time on the formation of the $ZnWO_4$ crystalline phase. Based on the crystallographic data of the known structure of $ZnWO_4$ (JCPDS code 15-0774), all the reflections of the product can be readily indexed as a pure monoclinic phase [space group: $P2/c$] of $ZnWO_4$.

In order to further demonstrate the formation process of $ZnWO_4$, the FT-IR spectra of the precursor treated at various temperatures were present in Fig. 2. The $ZnWO_4$ samples show main absorption bands at 450–1000 cm^{-1} [21]. The absorption bands with their maxima at 834 and 877 cm^{-1} can be due to the stretching modes of W–O in WO_6 octahedra [22]. The bands at 610 and 532 cm^{-1} were due to symmetrical vibrations of bridge oxygen atoms of the Zn–O–W groups. The absorption bands at 473 and 430 cm^{-1} can be assigned to symmetric and asymmetric deformation modes of W–O bonds and Zn–O bonds in WO_6 and ZnO_6 octahedra, respectively [21]. These vibrations could be identified to the synthesized $ZnWO_4$. It can be seen that $ZnWO_4$ crystalline phase formed, which is supported by the results of XRD analysis. Samples prepared at 400 and 450 °C exist terminal stretching mode band W–O_d at 985 cm^{-1} [23], but the intensity of this peak weakened with increase of calcination temperature, and then disappeared at 500 °C. This can be also explanation that the sample prepared at 400 °C shown in Fig. 1(a) was intergradation of $ZnWO_4$. The bands located at 2925 cm^{-1} due to the stretching modes of CH_2 group at CH_3CH_2OH, and that at 1455 cm^{-1} due to the bending mode of CH_2 group. The bands in the 3400 cm^{-1} region exhibit a strong absorption band, which is assigned to the (H stretching vibrations), the bands at 1630 cm^{-1} are assigned to the HOH bending vibrations. It is also evident that the samples prepared contain a significant amount of surface-adsorbed water and some structural water. Obviously, the O–H stretching vibrations decrease from the FT-IR measurements when temperature is increased to 550 °C. It indicates that the surface absorbed water decreases with the decrease of surface areas (Fig. 5(a)).

3.2. Grain size, morphology and surface area of $ZnWO_4$ photocatalyst

The variation of morphology and grain size of $ZnWO_4$ photocatalyst with temperatures and times could be found from the TEM and SEM results (Figs. 3 and 4). It can be seen from Fig. 3 that the morphological structure of $ZnWO_4$ obtained was homogenous. The grain size of $ZnWO_4$ increased when the temperature increased. At 450 °C for 4 h, it was about 200 nm. The grain size was much larger (about 400–500 nm) when the sample was calcined at 500 °C for 4 h and even larger (about several micrometers) when the temperature was 600 °C. The SEM images showed the aggregation and sintering between the particles more distinctly in Fig. 3(e). From the TEM and SEM images, we can conclude that a higher temperature the tendency of particles interconnected with each other and aggregated to the bigger particles is more significant. The influences of calcination time on the morphology of $ZnWO_4$ were shown in Fig. 4. It can be found that the grain size of $ZnWO_4$ powder grew up

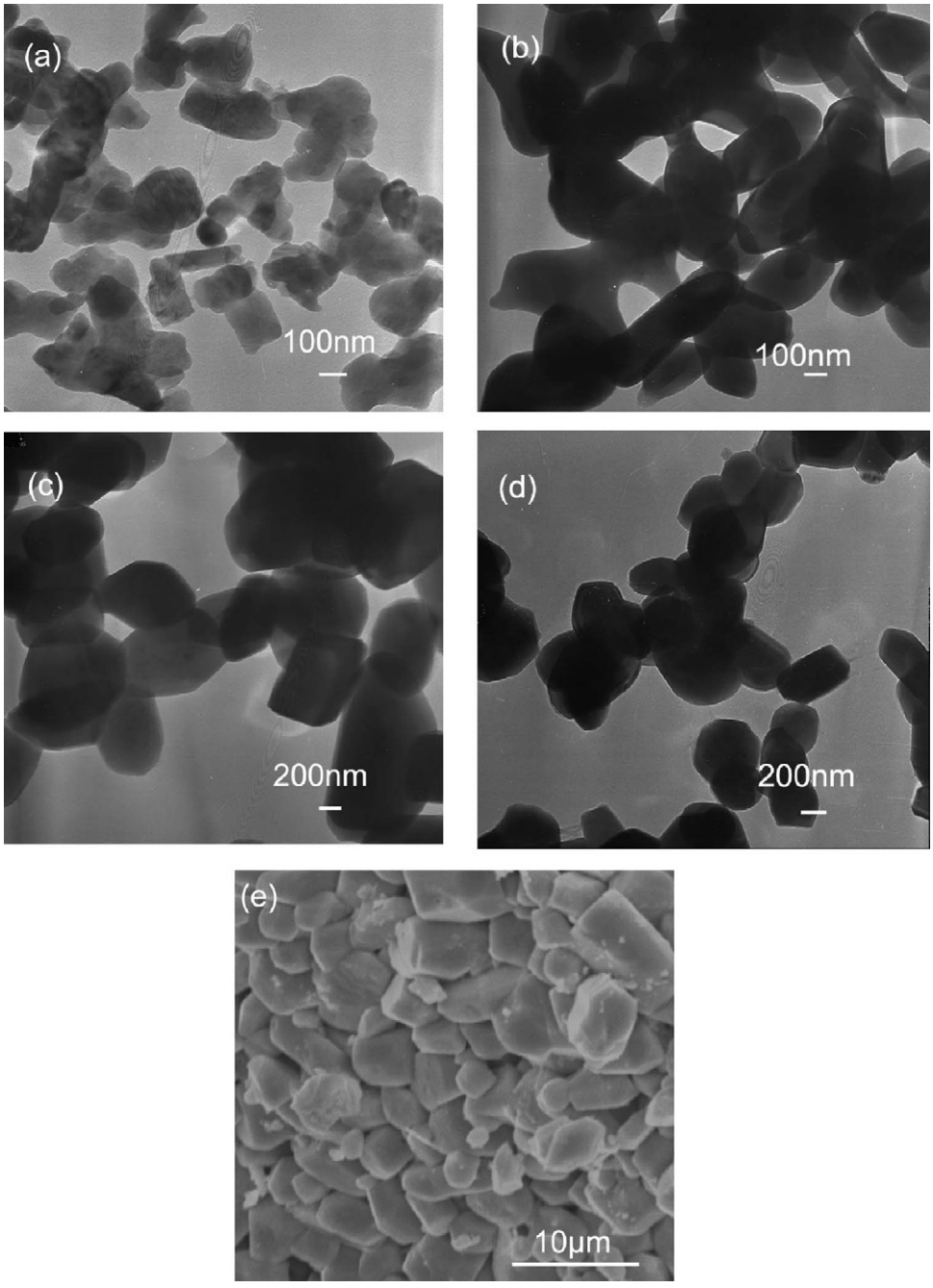

Fig. 3. Images of $ZnWO_4$ powder at various temperatures for 4 h: (a) 400 °C; (b) 450 °C; (c) 500 °C; (d) 550 °C; (e) 600 °C. (a)–(d) are the TEM morphology of the as-prepared samples, (e) is the SEM morphology of the $ZnWO_4$ powder.

from 300 to 800 nm with prolonging of calcination time from 1 to 16 h at 500 °C. It mildly rises as calcination time increased.

In Fig. 5, the relation between calcination treatment and specific surface area was shown. It can be seen from Fig. 5(a) that the surface areas of these catalysts decreased from 19.20 to 0.76 m^2/g in the range of 400–600 °C. These results indicate that calcination treatment improve the crystallinity of $ZnWO_4$ associated with crystal growth. This crystallinity improvement causes the decrease in surface area. From Fig. 5(b), it has to be mentioned that the surface areas of these catalysts only decreased 2.8 m^2/g (from 6.98 to 4.17 m^2/g) when the calcination time was prolonged from 1 to 16 h, indicating that calcination temperature played much more important role on surface areas of these catalysts. Meanwhile, the influence of time and temperature on surface area seems to be consistent with the results of XRD, TEM and SEM observation.

3.3. Photo-absorption properties

It is well-known that light absorption of the material and the migration of the light induced electrons and holes are the most key factors controlling photocatalytic reaction, which is rele-

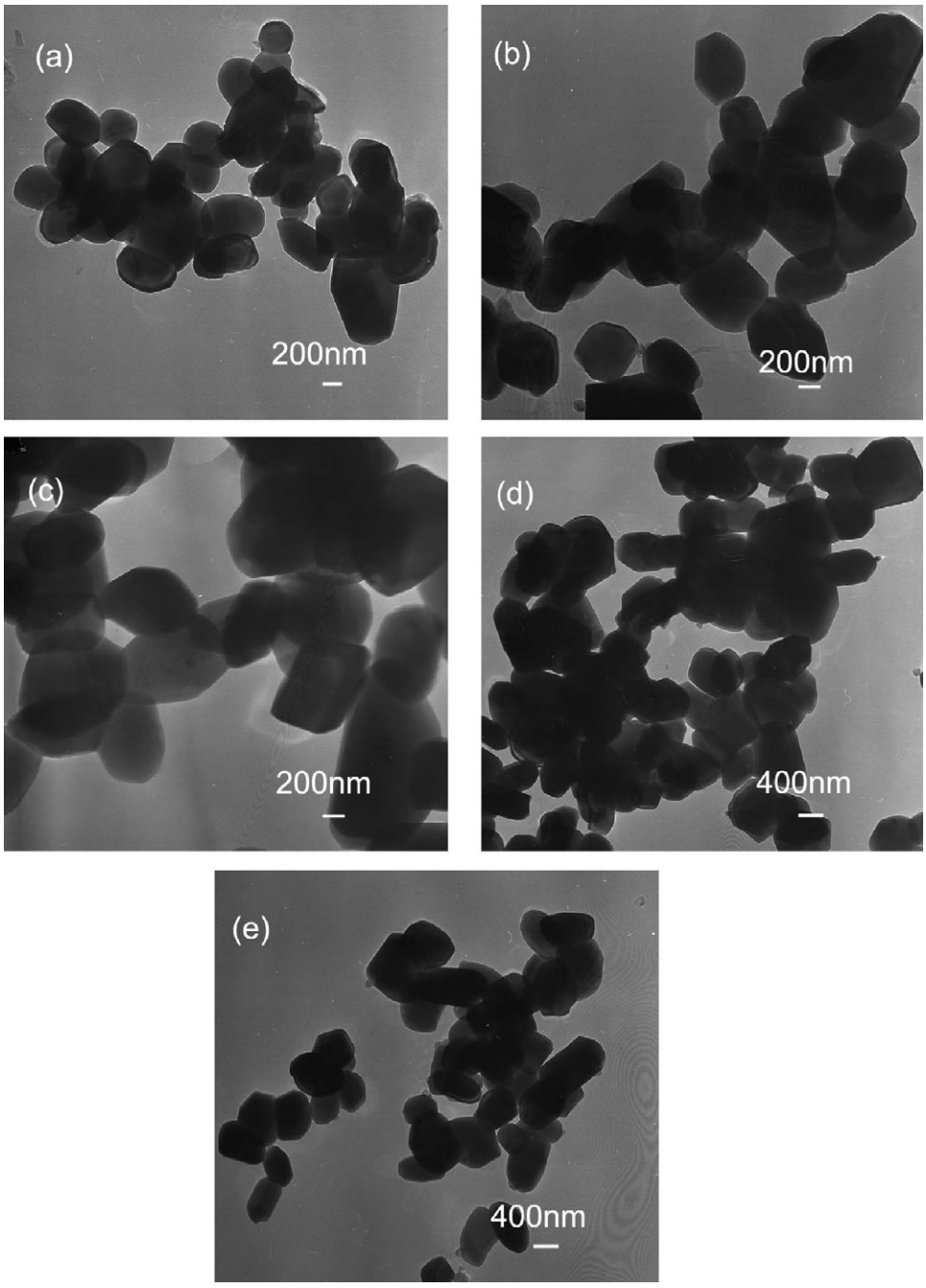

Fig. 4. TEM images of the as-prepared samples at 500 °C for various times: (a) 1 h; (b) 2 h; (c) 4 h; (d) 8 h; (e) 16 h.

vant to the electronic structure characteristics of the material [24,25]. Fig. 6 shows the result of diffuse reflection spectra of $ZnWO_4$ prepared at 500 °C for 4 h. This photocatalyst presented the photo-absorption properties in the UV light region at 380 nm. As shown in Fig. 6, the as-prepared $ZnWO_4$ shows three transition bands at 305 nm, 260 nm and 220 nm that correspond to the transition energy of 4.06 eV, 4.76 eV and 5.63 eV, respectively. According to the research of Nedilko and Hizhnyi [26], these transitions can be identified in the tungstate group.

For a crystalline semiconductor, it was shown that optical absorption near the band edge follows [27] $\alpha h\upsilon = A(h\upsilon - E_g)^{n/2}$, where α, υ, E_g, and A are absorption coefficient, the light frequency, the band gap, and a constant, respectively. Among them, n decides the characteristics of the transition in a semiconductor. According to the equation, the value of n for $ZnWO_4$ was 1 from the date in Fig. 6. The band gap of the photocatalyst was estimated to be 3.02 eV from the onset of the absorption edge. For W-based semiconductors, it was already found that excitons are formed due to the transitions into the tungstate W_{5d} states hybridized with O_{2p} and possess a very strong tendency for self-trapping [28]. Free electrons and holes can be created due to the transitions into cationic states. An active photocatalyst for the decomposition of the organic compounds must have a VB with strong oxidizing ability and photogenerated holes with

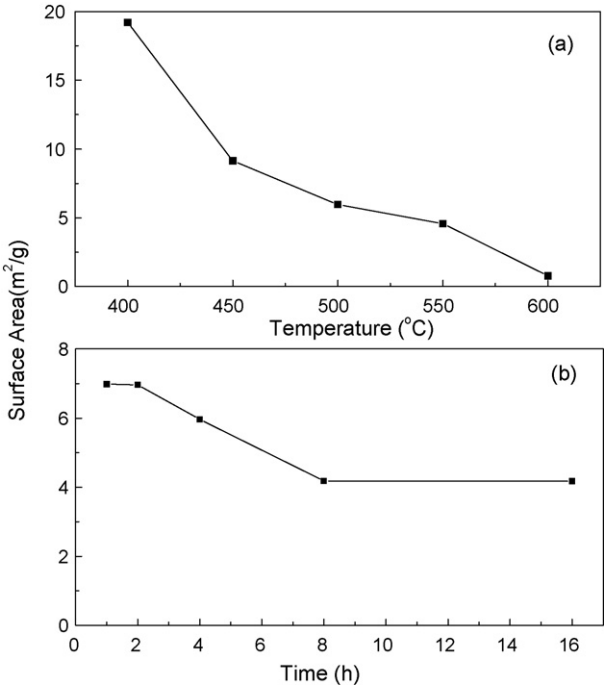

Fig. 5. Effect of calcination on the surface area of $ZnWO_4$: (a) various temperatures; (b) various times.

high mobility. The hybridized VB of $ZnWO_4$ has shown strong ability to photocatalytic degradation of the organic pollutants in the work described herein.

3.4. Photocatalytic performance

The photocatalytic activities of the obtained samples were evaluated by the decomposition of formaldehyde. In Fig. 7, the removal efficiency $R(\%)$ of formaldehyde in gaseous phase was shown. Calcination temperature is especially important for completing the crystallization. However, very high calcination temperature results in aggregation and decrease of surface area [29]. The results in Fig. 7(a) demonstrated that the photocatalytic activity is strongly dependent on the calcination

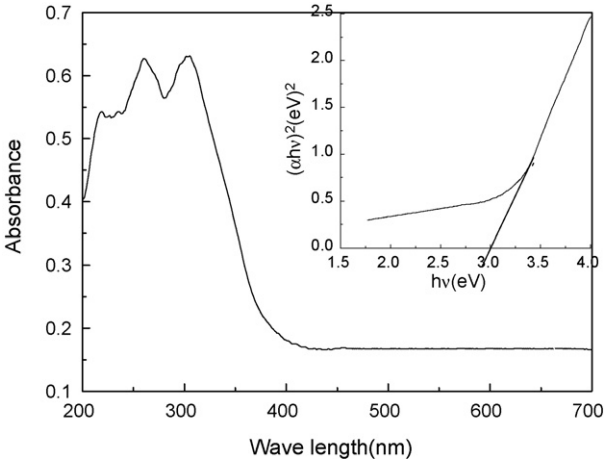

Fig. 6. Optical absorption of $ZnWO_4$ prepared at 500 °C for 4 h.

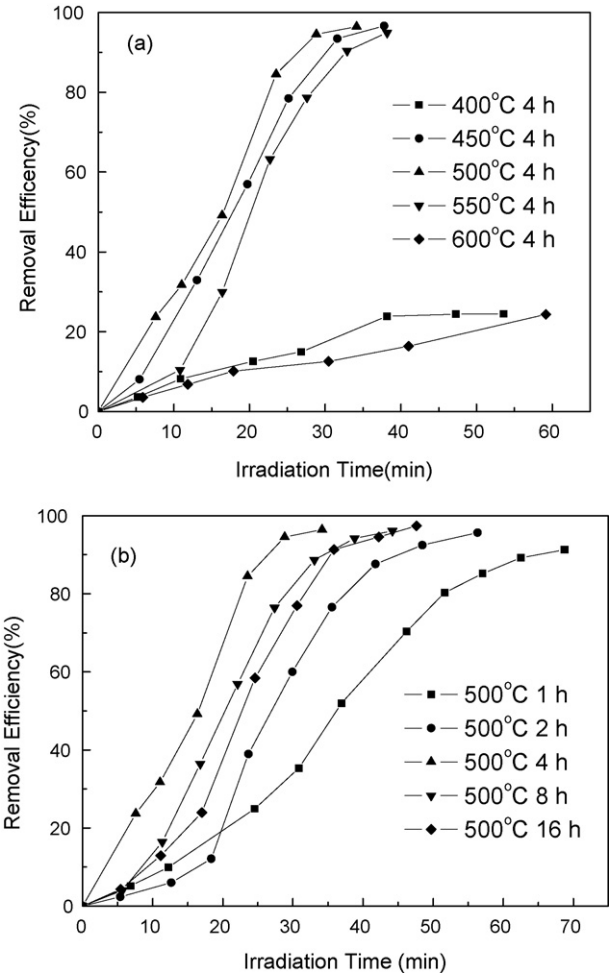

Fig. 7. Photo-decomposition of formaldehyde for the as-prepared samples calcined: (a) various temperatures; (b) various times.

temperature. With increase of calcination temperature, the photocatalytic activity of $ZnWO_4$ increased, which is due to the enhancement of $ZnWO_4$ crystallization. At 500 °C, $ZnWO_4$ photocatalyst reaches the highest photocatalytic activity with formaldehyde removal efficiency of 90% in 25 min. However, with further increasing of calcination temperature, the formaldehyde removal efficiency decreases from 93.2% to 10.8% in 25 min. The sample prepared at 600 °C showed only little photocatalysis efficiency to decompose formaldehyde. Those calcined above 500 °C have lower photocatalytic activities because of lower surface area and larger crystallite size. Namely, the larger the particle and grain size grow, the longer distance the electron–hole pairs have to migrate. In addition, the larger particle size resulted from lower absorptive capacity of formaldehyde on the surface of $ZnWO_4$ particles also abated its photocatalytic ability. At 400 °C, as-prepared $ZnWO_4$ possessed the largest surface area. Nevertheless, the broad XRD feature as shown in Fig. 1(a) demonstrated that crystallization of $ZnWO_4$ treated at 400 °C was incomplete. The amorphous is known to have very low photocatalytic efficiency compared to that of fine crystallinity due to an increased electron–hole recombination rate; hence the sample treated at 400 °C exhibited lower photocatalytic activity than that of sample calcined at a higher

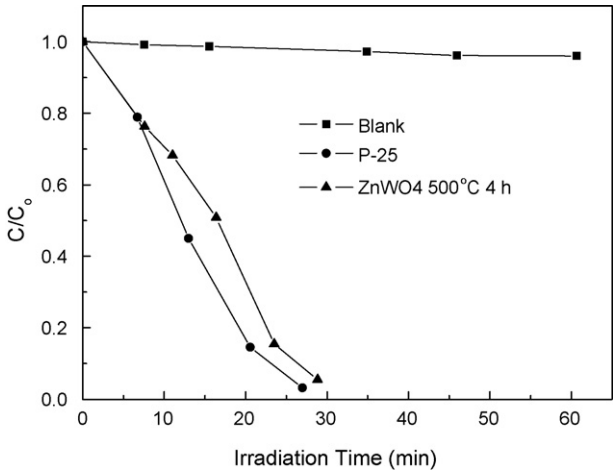

Fig. 8. Formaldehyde concentration changes over $ZnWO_4$ and P-25. Initial concentration of formaldehyde, 1200 ppm, catalyst loading, 50 mg.

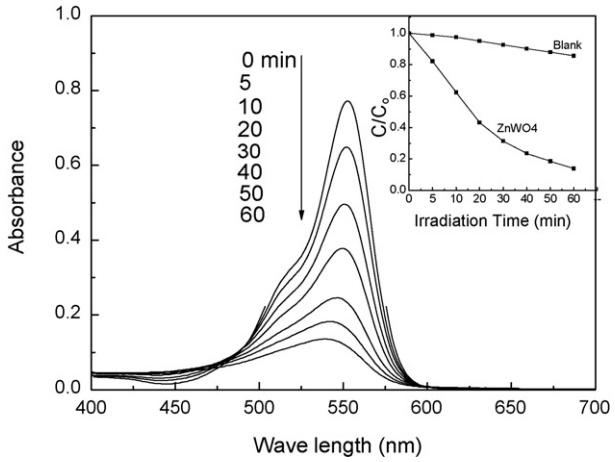

Fig. 9. UV–vis spectral changes of RhB (1×10^{-5} M) in aqueous solution $ZnWO_4$ dispersion as a function of irradiation time. Inset: RhB concentration changes over $ZnWO_4$ prepared at 500 °C for 4 h.

temperature. Thus the photocatalytic activity reaches a maximum at calcination temperature of 500 °C.

Fig. 7(b) shows the photocatalytic activity of $ZnWO_4$ powders obtained at 500 °C for different times. With increase of calcination time, the photocatalytic activity increased, and then decreased. The highest photocatalytic activity was got at the time of 4 h, which is supported by the results of the TEM (Fig. 4), BET (Fig. 5) and XRD (Fig. 1(b)) analysis. Prolonging the calcination time is an effective route to promote the crystallization of $ZnWO_4$ powders, and improve its photocatalytic activity. However, the particle size increased also, which lead to the low specific surface area and then decreased the photocatalytic activity of $ZnWO_4$ powder.

Fig. 8 plots the concentration changes of formaldehyde as a function of reaction time of the $ZnWO_4$ samples prepared at 500 °C for 4 h. It is amazing that over 90% of formaldehyde was photocatalytically degraded after 20 min irradiation. With increase of irradiation time, the concentration of formaldehyde in the reaction system decreased. In comparison, formaldehyde decomposition over P-25 was also carried out under the same conditions. As shown in Fig. 8, the photocatalytic activity of P-25 is slightly higher than that of as-prepared $ZnWO_4$ photocatalyst. For the decomposition of gas-phase compounds, this is due to two factors, which are the adsorption of gas molecules onto the photocatalyst surface and the photocatalytic decomposition of the absorbed organic molecules. The first factor is mostly governed by specific surface area. The second factor depends on light absorption property and rate of e^-–h^+ recombination. In our work, the irradiated area is the same, and the amount of photons absorbed by $ZnWO_4$ (3.02 eV) catalyst is slightly more than that of P-25 (3.2 eV). Therefore, in the decomposition of coated formaldehyde, the major factor is decomposition of the absorbed formaldehyde [30]. P-25 (55 m^2/g) has a higher affinity for the adsorption of formaldehyde but a lower photocatalytic degradation activity, whereas $ZnWO_4$ (6 m^2/g) has a higher photocatalytic degradation activity but a lower affinity for formaldehyde adsorption. As a result, the apparent removal of formaldehyde is almost similar between P-25 and $ZnWO_4$ systems. The blank experiment was also performed. It can be found that formaldehyde was almost not decomposed in the absence of $ZnWO_4$ photocatalyst under the same irradiation time, indicating that the presence of $ZnWO_4$ photocatalyst played an important role in the decomposition of formaldehyde.

The evaluation of photocatalytic activity was further carried out in aqueous solution for degradation of RhB. The temporal evolution of the spectral changes during the photo-degradation of RhB over $ZnWO_4$ prepared at 500 °C for 4 h was displayed in Fig. 9. Tetraethylated rhodamine shows a major absorption band at 553 nm. UV light irradiation of the RhB/$ZnWO_4$ dispersion leads to an apparent decrease in absorption peaks. The color of the dispersion disappeared after 80 min irradiation, indicating that at least the chromophoric structure of the RhB was destroyed. Comparison of the spectra after 60 min of irradiation with the initial one shows that approximately 80% of RhB was degraded through the destruction of the conjugated structure. The inset of Fig. 9 showed the temporal concentration changes of RhB. For comparison, the blank experiment was also performed. It can be also found that $ZnWO_4$ photocatalyst played an important role in the photo-degradation of RhB.

4. Conclusion

$ZnWO_4$ was successfully synthesized via precipitated process. The results of XRD and FT-IR proved that the monoclinic crystalline phase of $ZnWO_4$ was formed at 450 °C for 4 h and became perfect above 500 °C for 4 h. At 500 °C for 4 h, the photocatalyst reaches the highest photocatalytic activity with formaldehyde removal efficiency of 90% within 25 min. After 60 min of irradiation, $ZnWO_4$ photocatalyst shows that approximately 80% of RhB was degraded through the destruction of the conjugated structure. The large surface area and high crystallinity are responsible for its high photocatalytic activity. This method has the potential use in preparation of other complex oxide photocatalysts powders.

Acknowledgements

This work was partly supported by Chinese National Science Foundation (20433010, 20571047).

References

[1] R. Asahi, T. Morikawa, T. Ohwaki, K. Aoki, Y. Taga, Science 293 (2001) 269.
[2] M.R. Hoffman, S.T. Martin, W. Choi, D.W. Bahnemann, Chem. Rev. 95 (1995) 69.
[3] H. Yamashita, M. Harada, J. Misaka, M. Takeuchi, K. Ikeue, M. Anpo, J. Photochem. Photobiol. A: Chem. 148 (2002) 257.
[4] (a) J.M. Herrmann, J. Disdier, P. Pichat, J. Catal. 113 (1988) 72;
(b) D.S. Muggli, J.T. McCue, J.L. Falconer, J. Catal. 173 (1998) 470;
(c) X.Z. Li, F.B. Li, Environ. Sci. Technol. 35 (2001) 2381;
(d) D.S. Muggli, L. Ding, M.J. Odland, Catal. Lett. 78 (2002) 23.
[5] Y.F. Zhu, Y. Fang, M. Yi, Q.Y. Tian, J. Solid State Chem. 178 (2005) 224.
[6] A. Kudo, H. Kato, Chem. Lett. 26 (1997) 421.
[7] H. Kato, N. Matsudo, A. Kudo, Chem. Lett. 33 (2004) 1216.
[8] J.W. Tang, Z.G. Zou, J. Phys. Chem. B 107 (2003) 14265.
[9] J.W. Tang, Z.G. Zou, J.H. Ye, Catal. Lett. 92 (2004) 53.
[10] C. Zhang, Y.F. Zhu, Chem. Mater. 17 (2005) 3537.
[11] H.B. Fu, Y.F. Zhu, J. Phys. Chem. B 109 (2005) 22432.
[12] S. Yu, B. Liu, M. Mo, J. Huang, X. Liu, Y. Qian, Adv. Funct. Mater. 13 (2003) 639.
[13] P.F. Schofield, K.S. Knight, S.A.T. Redfern, G. Cressey, Acta Cryst. B53 (1997) 102–112.
[14] J. Ricote, L. Pardo, A. Castro, P. Millan, J. Solid State Chem. 160 (2001) 54.
[15] (a) H.B. Fu, J. Lin, L.W. Zhang, Y.F. Zhu, Appl. Catal. A: Gen. 306 (2006) 58–67;
(b) G.L. Huang, C. Zhang, Y.F. Zhu, J. Alloys. Compd. 432 (2007) 269–276.
[16] (a) X. Zhao, Y.F. Zhu, Environ. Sci. Technol. 40 (2006) 3367;
(b) X. Zhao, W.Q. Yao, S.C. Zhang, H.P. Yang, Y.F. Zhu, J. Solid State Chem. 179 (2006) 2562–2570.
[17] (a) S.J. Chen, J.H. Zhou, Chem. Phys. Lett. 375 (2003) 185;
(b) J.C. Brice, P.A.C. Whiffin, Br. J. Appl. Phys. 18 (1967) 581;
(c) W. Jander, W. Wenzel, Z. Anorg. Allg. Chem. 240 (1941) 67.
[18] (a) A.R. Phani, M. Passacantando, L. Lozzi, S. Santucci, J. Mater. Sci. 35 (2000) 4879;
(b) B. Liu, S.H. Yu, L.J. Li, J. Phys. Chem. B 108 (2004) 2788.
[19] J. Yu, J. Solid State Chem. 178 (2005) 1968.
[20] X.F. You, F. Chen, J.L. Zhang, J. Sol–Gel Sci. Technol. 34 (2005) 181.
[21] V.V. Fomichev, O.I. Kondratov, Spectrochim. Acta 50A (1994) 1113–1120.
[22] V.I. Tsaryuk, V.F. Zolin, Spectrochim. Acta A57 (2001) 355–359.
[23] M. Gotic, M. Ivanda, S. Popovic, S. Music, Mater. Sci. Eng. B77 (2000) 193–201.
[24] J. Tang, Z. Zou, J. Ye, Angew. Chem., Int. Ed. 43 (2004) 4463.
[25] J. Tang, Z. Zou, J. Ye, Chem. Mater. 16 (2004) 1644.
[26] S.G. Nedilko, Yu.A. Hizhnyi, Phys. Stat. Sol. (c) 2 (2005) 481.
[27] M.A. Butler, J. Appl. Phys. 48 (1977) 1914.
[28] V. Nagirnyi, M. Kirm, A. Kotlov, A. Lushchik, L. Jonsson, J. Lumin. 102 (2003) 597.
[29] C. Su, B.Y. Hong, C.M. Tseng, Catal. Today 96 (2004) 119–126.
[30] (a) H. Kim, W. Choi, Appl. Catal. B 69 (2007) 127–132;
(b) Y.T. Kwon, K.Y. Song, W.I. Lee, G.J. Choi, Y.R. Do, J. Catal. 191 (2000) 192–199.